Effect of uniaxial deformation on the optical scattering losses of a semicrystalline fluorocopolymer

Karsten Eichhorn, Christian Sinn, and Manfred Dettenmaier

Both small- and wide-angle light scattering as well as transmission measurements have been used to investigate the optical scattering losses of a vinylidene difluoride–tetrafluoroethylene–hexafluoropropylene copolymer crystallized from the melt. The main origin of the scattering loss is the wide-angle light scattering from the spherulitic superstructure. Uniaxial deformation transforms this structure into a fiber morphology. The attenuation of fibers has been measured for light propagating both parallel and perpendicular to the orientation axis. For both directions, the attenuation decreases with increasing draw ratio. Annealing of the fibers while keeping their ends fixed is an effective method to reduce the attenuation further, to a low value as close to that of the melt.

Key words: Semicrystalline polymers, optical scattering losses, mechanical deformation, polymer optical fibers.

1. Introduction

Polymer optical fibers are of growing importance for signal transmission in short distance applications.[1,2] Their advantages compared with silica fibers are low production costs, good processability, and high flexibility that extends even to large core diameters, which allow simple and thus cost-effective coupling between two fibers.

Polymer optical fibers are typically designed as multimode fibers with a step-index profile. As the core material has a refractive index of n_K, and the cladding a smaller refractive index of n_M, light that couples into the fiber under an angle smaller than the acceptance angle $\Theta_{\max} = \arcsin({n_K}^2 - {n_M}^2)^{1/2}$ will be guided through the fiber by total internal reflection at the core–cladding interface.

The amplitude of guided light decreases along the fiber because of processes such as absorption and scattering in the bulk materials; imperfections of the core–cladding interface are not considered here. Absorption losses are due to molecular excitations and therefore depend on the chemical composition of the fiber, whereas scattering losses result from local fluctuations of the refractive index around its mean. These fluctuations in refractive index arise in turn from fluctuations in density, such as thermal density fluctuations in amorphous polymers or anisotropy, for example, those caused by the stacks of lamella in semicrystalline polymers.[3,4] The light scattered by such anisotropy fluctuations contains a depolarized component in contrast to the light scattered by density fluctuations, which maintain its polarization.

The core materials of commercially available polymer fibers typically are amorphous polymers such as poly(methyl methacrylate) (PMMA), polystyrene, and polycarbonate, all of which have excellent optical properties.[5] Semicrystalline fluorinated copolymers, which are used widely as cladding materials, exhibit high chemical resistance, thermal stability, and low refractive index. The typical attenuation of fibers with a PMMA core is some 100 dB/km at a wavelength of $\lambda = 650$ nm.[6] In contrast to amorphous materials semicrystalline polymers exhibit a significantly larger attenuation of some 100 dB/m, which is due to their morphology.

Here we report investigations on the scattering losses of a semicrystalline fluorinated copolymer, which show that uniaxial drawing of the samples is

K. Eichhorn is with Hella KG Hueck and Company, D-59552 Lippstadt, Germany. C. Sinn is with the Institut für Physik, Johannes-Gutenberg-Universität, Staudingerweg 7, D-55099 Mainz, Germany. M. Dettenmaier is with the Max-Planck-Institut für Polymerforschung, Postfach 3148, D-55021 Mainz, Germany.

Received 23 October 1995.
0003-6935/97/184259-06$10.00/0

effective in drastically reducing the attenuation of melt-crystallized samples.[7]

2. Experiment

A. Characterization of the Sample Material

Our investigations were conducted on a statistical fluorinated copolymer consisting of the monomer units vinylidene difluoride (36.5 mol. %), tetrafluoroethylene (52 mol. %), and hexafluoropropylene (11.5 mol. %). For brevity we refer to this copolymer as VTH.

The semicrystalline VTH exhibits a glass transition at approximately 0 °C, as revealed by differential scanning calorimetry, and a broad melting range from 80 to 140 °C with a maximum at 125 °C. The heat of fusion amounts to approximately 10 J/g. The macroscopic density has been measured to $\rho = 1.940 \pm 0.003$ g/cm^3. The degree of crystallinity determined by wide-angle x-ray scattering is approximately 10% and remains constant during sample preparation.[8] The refractive index at 20 °C is $n = 1.364 \pm 0.002$.

B. Sample Preparation

The copolymer was provided by Hoechst AG, Gendorf, Germany, in granular form. The granules were molten at a temperature of 165 °C under a pressure of 5 MPa. The highly viscous melt was annealed for a few hours at 140 °C and then cooled to room temperature at a cooling rate of 4.5 K/min. Dumbbell-shaped specimens were drawn with a tensile testing machine using different drawing temperatures in the interval of 60 °C $\leq T_S \leq$ 80 °C and a nominal strain rate of 4×10^{-4} s^{-1}. Finally, the samples were quenched to room temperature using compressed air. The draw ratio $\lambda_S = L/L_0$ is defined as the ratio of the sample lengths after and before deformation. The final sample size was approximately 10 mm × 2 mm × 2 mm. The uniaxial deformation state of the samples was controlled by two-dimensional wide-angle x-ray scattering. The accessible range of drawing temperatures was limited to 60 °C $\leq T_S \leq$ 80 °C. In fact, samples stretched at $T_S \leq 40$ °C showed intensive stress whitening because of crack formation. Inside the melting region ($T_S \geq 100$ °C) stretching was accompanied by flow of the material. After drawing, one sample was annealed with fixed ends. The traverse was halted at the desired draw ratio and the temperature was raised to the annealing temperature of $T_A = 105$ °C.

C. Optical Apparatus

Light transmission measurements were performed using the setup shown in Fig. 1(a). The melt-crystallized samples were placed in a glass cell filled with ethanol. Because ethanol serves as a refractive-index matching liquid, the contributions from both scattering and reflections at the surface of the sample are less than 0.03%, which is negligible for evaluation of the scattering losses. A heatable

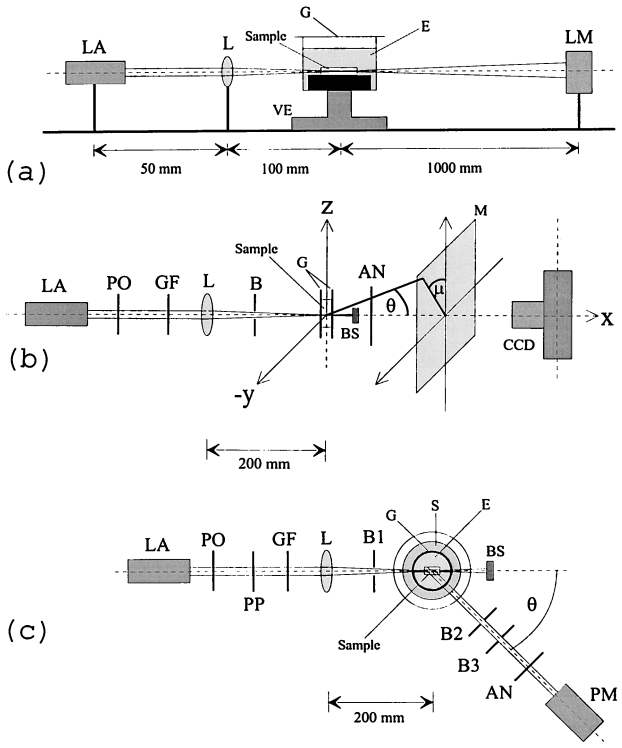

Fig. 1. Sketches of the different experimental setups. (a) Transmission measurement: LA, laser; L, lens; E, immersion bath (ethanol); G, glass cell; VE, translation unit; LM, photodiode. (b) Small-angle light scattering: PO, polarizer; AN, analyzer; B, aperture; BS, beam stop; M, screen; CCD, detector; *xyz*, laboratory frame, μ, azimuthal angle; θ, scattering angle. (c) Wide-angle light scattering: PP, phase plate; GF, gray wedge; S, immersion bath (silicon oil); PM, photomultiplier.

sample chamber without immersion liquid was employed to measure molten material. The cell was mounted on a translation stage allowing for the displacement of the sample parallel and perpendicular to the light beam. An unpolarized He–Ne laser ($\lambda = 632.8$ nm) was used as the light source. The laser light was focused by a lens ($f = 100$ mm) into the center of the sample, and the transmitted light was detected by a large-area photodiode.

In addition to the transmitted beam, the detector receives light that is scattered under small angles ($\theta \leq 0.5°$ for our setup). However, the fact that Lambert's law [Eq. (1) below] is valid for all samples, even those that scatter very strongly, demonstrates that the contribution from scattering is negligible. Small-angle light-scattering measurements were performed as illustrated in Fig. 1(b). The setup is similar to that described above. The polarized He–Ne laser was focused into the sample film, which was held between two glass plates. The scattered light passed through a rotatable analyzer, which enabled measurements in different polarization geometries. A beam stop prevented the transmitted beam from reaching the screen. The scattering pattern was recorded by a CCD camera.

The wide-angle light-scattering measurements were conducted by using a standard light-scattering

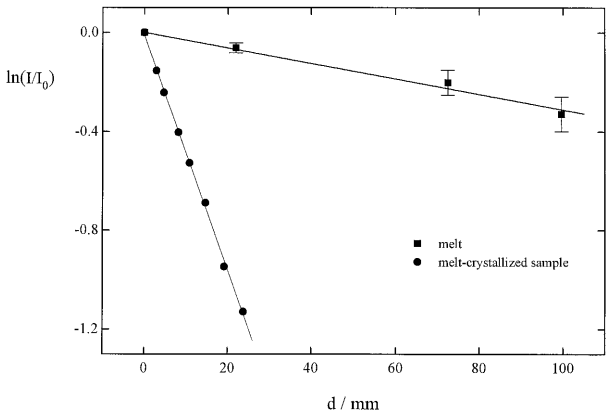

Fig. 2. Light transmission of a molten sample and a melt-crystallized sample as a function of sample thickness.

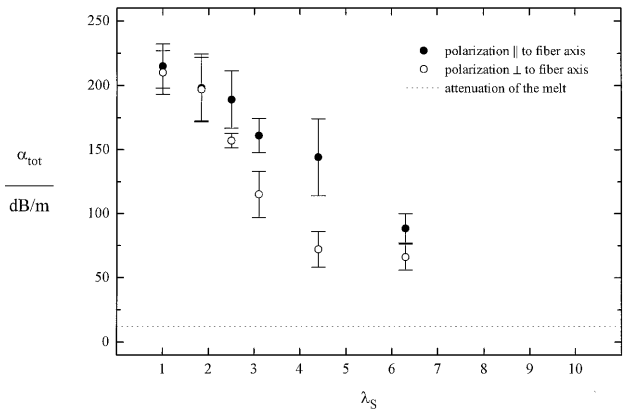

Fig. 3. Attenuation of drawn samples determined by light transmission measurements perpendicular to the fiber axis as a function of draw ratio λ_S. Data are given for polarization parallel and perpendicular to the fiber axis.

goniometer. A sketch of the setup is shown in Fig. 1(c), which is a projected view onto the scattering plane. The light source was a Spectra-Physics Kr^+ laser ($\lambda = 647.1$ nm). The laser light was polarized perpendicular to the scattering plane. The direction of polarization could be rotated by means of a $\lambda/2$ plate. A second polarizer was used to analyze the polarization of scattered light. Polarizer and analyzer were kept either vertical or horizontal to the scattering plane to measure the different scattering components I_{VV}, I_{VH}, I_{HV}, and I_{HH}. The intensity of the scattered light in an unpolarized experiment can then be evaluated by summing over these components. Absolute intensities were obtained by calibrating the apparatus with toluene. The disturbing speckle pattern was suppressed by moving the sample vertically, applying the method described in detail by Eichhorn and Sinn.[9]

3. Results and Discussion

A. Transmission Measurements

The absorption spectrum of melt-crystallized samples exhibits a continuous decrease toward larger wavelengths in the range from 350 to 750 nm, with a λ^{-4} dependence typical for Rayleigh light scattering. This result shows that scattering is the main contribution to the attenuation of samples. Transmission measurements therefore provide information for both the total and scattering losses. Lambert's law states that the transmitted intensity I_t is given by

$$I_t = I_0 \exp(-md), \tag{1}$$

with the incident intensity I_0, the extinction coefficient m, and the sample thickness d. The attenuation coefficient α in decibels/length is then given by

$$\alpha = (10/\ln 10) \times m. \tag{2}$$

Figure 2 shows the results of transmission measurements of the VTH melt and a melt-crystallized sample. From the linear fit to the data points, the attenuation of the melt-crystallized sample is determined to be $\alpha = 210$ dB/m, whereas the melt exhibits an attenuation of $\alpha = 12$ dB/m. The attenuation of the melt is considerably higher than the theoretical value of $\alpha \approx 0.1$ dB/m, which is calculated under the assumption that scattering only from thermal density fluctuations contributes to the loss.[4] We therefore conclude that the attenuation of the melt is governed by impurities such as catalyst and dust particles, which are difficult to remove because of the high viscosity of the melt. This conclusion is supported by the strong angular dependence of scattered light, which is shown in Fig. 7. Because the same impurities also contribute to the scattering of the copolymer after crystallization, the attenuation of the melt represents the minimum that melt-crystallized samples can exhibit.

The attenuation of VTH drawn to fibers decreases with increasing deformation, both parallel and perpendicular to the draw axis. Figure 3 shows the results for light propagating perpendicular to the fiber axis and for each of the two cases that the polarization of the incident beam is either perpendicular or parallel to the draw axis. The samples were drawn at $T_S = 60$ °C. In both cases, the attenuation de-

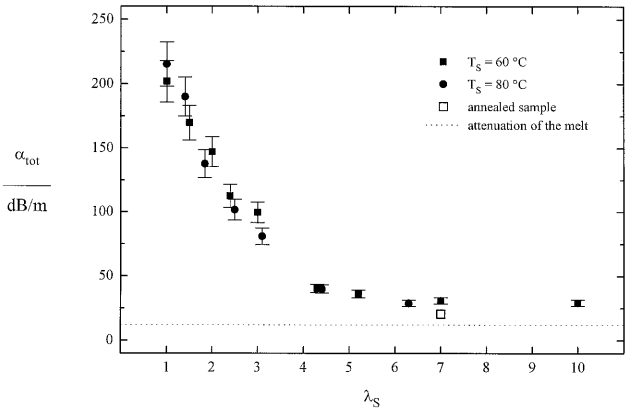

Fig. 4. Attenuation of drawn samples determined by light transmission measurements parallel to the fiber axis as a function of draw ratio λ_S for two different stretching temperatures T_S.

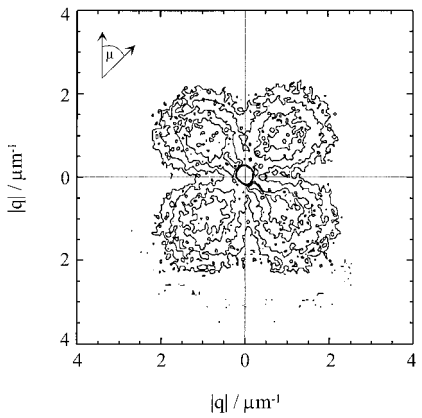

Fig. 5. Depolarized small-angle light-scattering pattern of a melt-crystallized sample as a function of q.

creases from 210 dB/m for the undrawn sample to approximately 80 dB/m at high draw ratios (λ_S = 6.3). The initial decrease is stronger if the polarization is perpendicular to the fiber axis. This effect has already been described by Stein *et al.*[10,11] for thin films of polyethylene. Technical applications have made use of the increase in transparency perpendicular to the preferential direction, e.g., in the production of transparent semicrystalline films.[12]

Applications of the material in optical fibers, however, require a low attenuation for light propagating parallel to the fiber direction. Figure 4 shows the attenuation in this direction for samples with different draw ratios drawn at 60 °C and 80 °C. The attenuation strongly decreases for each of the two drawing temperatures. At high draw ratios, the attenuation reaches a limit of approximately 28 dB/m. This value is only a factor of ~2 higher than the attenuation of the melt.

B. Small-Angle Light-Scattering Measurements

Semicrystalline polymers consist of a complex spatial arrangement of amorphous and crystalline phases. Their basic morphologic entities are thin crystalline lamellae separated from each other by amorphous layers. In a spherulite, the lamellae radiate from the center and branch sufficiently often to occupy the outwardly increasing volume, which can also be filled by additional amorphous material. The structure generated by this process may be thought of as an optically anisotropic sphere with radially and transversally different refractive indices.[13]

Like most polymers crystallized from the melt, VTH exhibits such a spherulitic superstructure, which leads to an intensive scattering of light and therefore to a strong attenuation of the melt-crystallized sample. Figure 5 shows the depolarized small-angle light scattering of VTH in a plane perpendicular to the laser beam. The scattering intensities are plotted as a function of $q = 4\pi/\lambda \times \sin(\theta/2)$, where θ is the angle between the wave vector of the incident and scattered light. The measured four-leaf-clover pattern, which is characteristic for the scattering of spherulites, can be described quantitatively by the theory of Stein and Rhodes.[14] The mean radius of the spherulites calculated from the scattering maximum at q_{max} is R = 2.7 μm.

To study the deformation of the spherulites the fiber axis was oriented perpendicular to the incident laser beam. The scattering patterns are in qualitative agreement with the predictions of Samuels.[15] Figures 6(a) and 6(b) show depolarized small-angle light-scattering results of samples with low (λ_S = 1.4) and medium (λ_S = 3.1) deformation ratios, respectively. The microscopic deformation ratio λ_M calculated from the position of the scattering maxima is smaller than λ_S (λ_M = 1.0 and λ_M = 1.8) indicating that the deformation is nonaffine.

In the low-angle range, the measurements do not provide precise quantitative information on the scattering losses. However, integral intensities have been estimated from scattering patterns such as those shown in Figs. 5, 6(a) and 6(b) for the depolarized component. The results indicate that the losses decrease slightly with increasing draw ratio of the material.

C. Wide-Angle Light-Scattering Measurements

Wide-angle light scattering provides valuable quantitative information on the scattering losses of light propagating parallel to the fiber axis. Because of

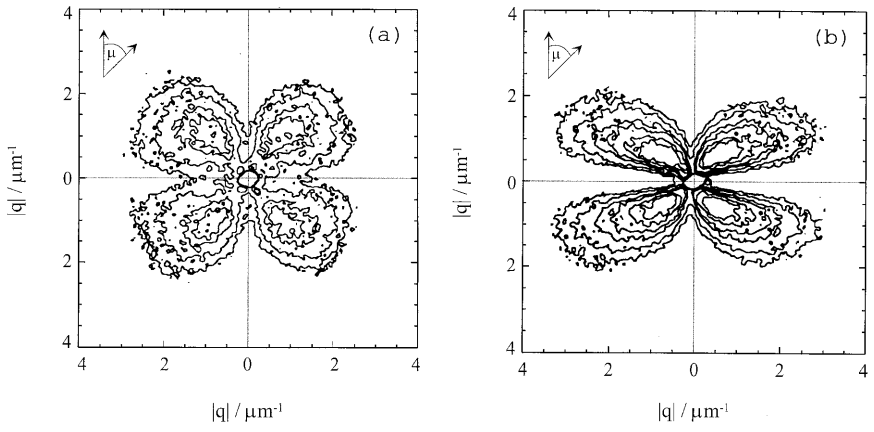

Fig. 6. Depolarized small-angle light-scattering patterns of drawn samples for two different deformation ratios as a function of q; the incident light was perpendicular to the fiber axis. (a) λ_S = 1.4, λ_M = 1.0; (b) λ_S = 3.1, λ_M = 1.8.

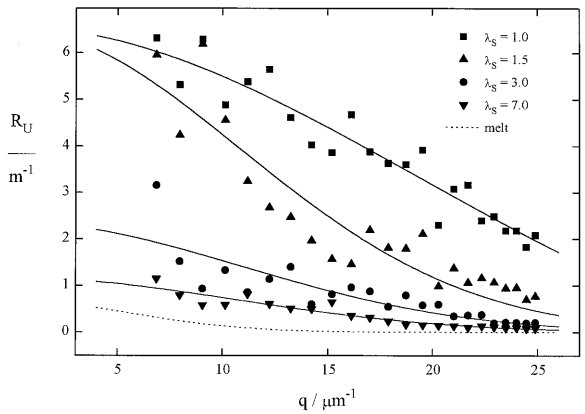

Fig. 7. Rayleigh ratio for unpolarized light of melt-crystallized samples as a function of q; the incident light was parallel to the fiber axis. Parameter is the draw ratio λ_S; the drawn curves are fits of a Debye function to the data points.

the birefringence of the samples, the quantitative analysis is more complicated for light propagating perpendicular to the fiber axis. In the q range accessible by wide-angle light scattering the scattering pattern is isotropic. The results can be used to interpret the data in Fig. 4. Figure 7 shows the Rayleigh ratio

$$R_U = (I_S/I_0)(a^2/V) = 1/2(R_{VV} + R_{VH} + R_{HV} + R_{HH}) \quad (3)$$

parallel to the fiber axis as a function of draw ratio; I_S and I_0 are the intensities of unpolarized scattered and incident light, respectively; a is the distance between the scattering volume V and the detector. R_U drastically decreases with increasing draw ratio.

Wide-angle light scattering probes fluctuations of the refractive index with correlation lengths small compared to the mean radius of the spherulites. To obtain the scattering losses caused by these fluctuations, a Debye function $R_U = a(1 + bq^2)^{-2}$ was fitted to the data of Fig. 7 and subsequently integrated numerically between 0° and 180°. The results are presented in Table 1 together with the data determined by transmission measurements. It is clearly seen that the attenuation of melt-crystallized and oriented samples is governed by scattering losses in the wide-angle range which originate from inhomogeneities within the spherulites. A detailed analysis of the contributions from the different polarization geometries shows that the decrease in scattering losses is due mainly to anisotropy fluctuations, whereas the contributions that are due to density fluctuations remain almost constant as a function of draw ratio.[7]

Table 1. Attenuation Determined by Wide-Angle Light Scattering (α_s) and Transmission Measurements (α_{tot}) as a Function of Draw Ratio λ_S

λ_S	1.0	1.5	3.0	7.0	10.0
α_s/dB m^{-1}	195	118	47	19	20
α_{tot}/dB m^{-1}	210	170	100	31	29

Model calculations indicate that the decrease in scattering losses parallel to the draw axis results from the orientation of the crystalline scattering units (stacks of lamellae), whereas the decrease in scattering losses perpendicular to the fiber axis is due to the reduced contrast between the scattering units and their surroundings. Details of these investigations, together with an analysis of the angular dependence of the wide-angle light scattering, will be presented in a forthcoming paper.

D. Effect of Annealing

The results presented in Subsections 3.A–3.C demonstrate that drawing considerably reduces the attenuation of melt-crystallized samples. Since thermal treatment can strongly affect the physical properties of polymer fibers, attention has been given to the scattering losses of drawn and subsequently annealed samples. Depending on whether the fibers are annealed with free or fixed ends, one can observe two different effects. Annealing with free ends increases the attenuation. The results obtained are in good agreement with the data in Fig. 4 provided the draw ratio is reduced by the amount of shrinkage.

Under appropriate conditions, annealing with fixed ends, however, reduces the attenuation further. This is demonstrated in Fig. 4, where data are included for a sample that has been annealed for 30 min at 105 °C. The attenuation of this sample is only 18 dB/m, which is close to the value measured for the melt. The effect of annealing depends strongly on both the annealing temperature and the draw ratio of the fibers. For example, fibers with either a much lower draw ratio or annealing temperature do not exhibit any significant change in attenuation.

4. Conclusion

The spherulitic superstructure of melt-crystallized VTH results in light-scattering losses. To reduce these losses samples have been deformed uniaxially. Transmission measurements demonstrate that the attenuation decreases strongly with increasing draw ratio. Both small- and wide-angle light scattering have been used to study the transformation of the spherulitic structure into a fiber morphology. The change in the small-angle scattering pattern clearly reflects the deformation of the spherulites. A drastic decrease in intensity is, however, observed only in the wide-angle range indicating that the light-scattering losses are due to fluctuations of the refractive index at distances small compared to the radius of the spherulites. These fluctuations are attributed to the stacks of lamellae that build up the spherulitic structure.

One can reduce the attenuation of VTH further by annealing fibers with fixed ends. The values obtained are close to the attenuation of the melt. The results presented in this paper are relevant to the application of semicrystalline polymers in optical fibers. It can be concluded that the potential of these

polymers as cladding or even core material is greater than previously assumed.

This research was supported by the Bundesministerium für Bildung, Wissenschaft, Forschung und Technologie. M. Dettenmaier gratefully acknowledges funds from the Fonds der Chemischen Industrie. This study benefited greatly from the fruitful collaboration with T. Dittmer, Hoechst AG.

References

1. R. M. Glen, "Polymeric optical fibre," Chemtronics **1,** 98–106 (1986).
2. C. Emslie, "Review: polymer optical fibres," J. Mater. Sci. **23,** 2281–2293 (1988).
3. M. Dettenmaier, "Elastische Lichtstreuung an Polymeren," Progr. Colloid Polym. Sci. **66,** 169–181 (1979).
4. M. Dettenmaier, "Effect of structure on the scattering losses of polymer optical fibre materials," Chimia **47,** 397–401 (1993).
5. P. Herbrechtsmeier, "Polymere Lichtwellenleiter," Kunststoffe **79,** 1040–1044 (1989).
6. K. Eben, "Plastic optical fiber: yesterday–today–tomorrow," Fiberoptic Product News **12,** 17–19 (1992).
7. K. Eichhorn, "Untersuchungen zum optischen Streu- und Dämpfungsverhalten orientierter teilkristalliner Fluorcopolymere im Hinblick auf ihre Anwendung in Lichtleitern," dissertation (Cuvillier-Verlag, Göttingen, 1994).
8. H. Freimuth, C. Sinn, and M. Dettenmaier, "Structure and deformation behaviour of a vinylidene fluoride–tetrafluoroethylene–hexafluoropropylene terpolymer," Polymer **37,** 831–836 (1996).
9. K. Eichhorn and C. Sinn, "Suppression of the speckle noise in solid polymer samples: a light scattering study," Opt. Eng. **33,** 3368–3371 (1994).
10. F. H. Norris and R. S. Stein, "The scattering of light from thin polymer films. IV. Scattering from oriented polymers," J. Polym. Sci. **27,** 87–114 (1958).
11. R. S. Stein, J. J. Keane, F. H. Norris, F. A. Bettelheim, and P. R. Wilson, "Some light scattering studies of the texture of crystalline polymers," Ann. N.Y. Acad. Sci. **83,** 37–59 (1959).
12. R. S. Stein and R. Prud'homme, "Origin of polyethylene transparency," Polym. Lett. **9,** 595–598 (1971).
13. J. M. Haudin, "Optical studies of polymer technology," in *Optical Properties of Polymers*, G. H. Meeten, ed. (Elsevier, London, 1986), Chap. 4.
14. R. S. Stein and M. B. Rhodes, "Photographic light scattering by polyethylene films," J. Appl. Phys. **31,** 1873–1884 (1960).
15. R. J. Samuels, "Small-angle light scattering from deformed spherulites: theory and its experimental verification," J. Polym. Sci. Part C **13,** 37–53 (1966).